RESEARCH ARTICLE

Particle & Particle Systems Characterization
www.particle-journal.com

Water-Dispersible BODIPY Multifunctionalized Silicon Oxide Nanoparticles for Glutathione Sensing

*Saman Bagherpour, Patricia Vázquez, Mariano Redondo-Horcajo, Teresa Suárez, José Antonio Plaza, and Lluïsa Pérez-García**

Glutathione (GSH), a thiol containing small peptide, plays pivotal roles in maintaining cellular redox balance, metabolism, detoxification, and scavenging of free radicals. Aberrant GSH levels in cells and tissues are associated with various disorders, underscoring the importance of accurate GSH detection for clinical diagnosis and therapy monitoring. Several molecular probes have been designed as fluorescent-based GSH sensors. However, their water insolubility and the need of using organic cosolvents hinder their applicability on biological samples. Alternatively, nanomaterials have proven to be highly promising for boosting the precision of treatments and enhancing the accuracy of diagnosing diseases, thanks to their compatibility with biological environments and improved cell uptake. Here, the synthesis and characterization of a boron-dipyrromethene (BODIPY)-based probe (PB) are reported, incorporating a fluorescent BODIPY core, chlorine substituents for reaction with GSH, and a linking moiety for conjugation to the surface of silicon oxide nanoparticles (SONPs). Functionalized SONPs with PB are also characterized at the nanoscale using high-resolution transmission electron microscopy (HR-TEM), dynamic light scattering (DLS), Zeta potential, Fourier transform infrared spectroscopy (FTIR), thermogravimetric analysis (TGA), UV–Vis absorption, and fluorescence spectroscopies, confirming the surface functionalization and water-dispersibility of functionalized SONPs with PB. GSH sensing is evaluated in aqueous solution, conjugated to SONPs, and in living cells, showing promising potential for ratiometric GSH detection.

1. Introduction

Glutathione (GSH) is one of the most prevalent thiol-containing biomolecules in biological systems. It has been demonstrated that GSH performs crucial physiological tasks including preserving the cells' optimal redox environment, cell metabolism, detoxification, and free radical scavenging.[1] For healthy individuals, intracellular concentrations of GSH range from 0.5×10^{-3} to 10×10^{-3} M, and its concentrations in physiological fluids are approximately 2×10^{-6} to 12×10^{-6}.[2] At normal physiological condition, GSH levels are maintained at the functional range, but several disorders, including cancer, Alzheimer's, and heart disease, are linked to abnormal levels of GSH in cells.[3] Therefore, establishing scientific protocols to accurately and conveniently detect GSH is crucial for early clinical diagnosis, monitoring the course of a disease, and anticipating the outcome of therapy.[4]

A sensitive method for fluorescence detection of GSH is considered to be molecular imaging based on fluorescent probes.[5,6] For instance, Lim et al.[7] reported a heptamethine–azo conjugate as an off–on mitochondrial GSH probe.

S. Bagherpour, L. Pérez-García
Departament de Farmacologia
Toxicologia i Química Terapèutica
Universitat de Barcelona
Av. Joan XXIII 27-31, Barcelona 08028, Spain
E-mail: mlperez@ub.edu

The ORCID identification number(s) for the author(s) of this article can be found under https://doi.org/10.1002/ppsc.202400134

DOI: 10.1002/ppsc.202400134

S. Bagherpour, L. Pérez-García
Institut de Nanociència i Nanotecnologia IN^{2}UB
Universitat de Barcelona
Barcelona 08028, Spain

P. Vázquez, M. Redondo-Horcajo, T. Suárez
Centro de Investigaciones Biológicas Margarita Salas
CIB (CSIC)
Madrid 28040, Spain

P. Vázquez
Departamento de Bioquímica y Biología Molecular
Facultad de Medicina
Universidad Complutense de Madrid
Madrid 28040, Spain

J. A. Plaza
Instituto de Microelectrónica de Barcelona
IMB-CNM (CSIC)
Campus UAB, Cerdanyola del Vallès, Barcelona 08193, Spain

However, one of the most important issues for the in vitro applicability of molecular probes is their lack of water solubility, and the use of mixtures of organic solvents and water has led to the damage of cell tissues and unreliable results.[8]

On the other hand, nanostructured materials have also received a lot of interest thanks to notable characteristics such as high surface area, surface functionalization capability, physical resilience, and improved biocompatibility, igniting the investigation into using nanoparticles in biomedicine and nanobiosensors, which can overcome the limitations resulting from molecular probes.[9,10] For instance, Song et al. reported the preparation of functionalized carbon quantum dots (CQDs) with amino groups which can bind GSH via electrostatic interactions resulting in a change of fluorescence properties of CQDs.[11] Silicon oxide nanoparticles (SONPs) are also considered a promising category of porous nanomaterials with strong biocompatibility, controlled size, simple surface modification, and other properties that make them ideal for a range of biomedical applications.[12] By modifying SONPs to be water-soluble, incorporating a specific water-soluble dispersant and using a fluorophore sensitive to GSH, the resulting nanosensor can address the limitations associated with traditional molecular probes.[12,13]

Linkers with polyethylene glycol (PEG) or polyethylene oxide (PEO) moieties can significantly improve the water dispersibility of various substances, including nanoparticles due to its ether oxygen atoms, which can form hydrogen bonds with water molecules.[14,15] This affinity for water helps PEG-functionalized or PEO-functionalized nanoparticles to remain dispersed in aqueous environments rather than aggregating or precipitating out of solution. This modification can transform a hydrophobic surface into a more hydrophilic one, thereby improving its compatibility with water and enhancing dispersibility of nanoparticles used for imaging, therapy, and diagnostics.[16,17] The improved water dispersibility ensures that these nanoparticles can navigate the aqueous environments of the body efficiently.

In the current work, the boron-dipyrromethene (BODIPY)-based PB (Scheme S1, Supporting Information) has been chosen as the GSH probe because BODIPY scaffolds possess exceptional qualities such as desirable fluorescence quantum yield, photostability, and pH insensitivity. Moreover, PB incorporates chlorine substituents for reaction with GSH and a propargyloxy moiety at the para position of the meso phenyl substituent for conjugation to the SONPs surface. PB was synthesized and characterized by ^{1}H NMR, ^{13}C NMR and FT-IR spectroscopies, as well as mass spectrometry. The immobilization of PB on silicon oxide nanoparticles (SONPs-N3-PEO) was performed, and synthesized SONPs-N3-PEO were characterized using TEM, DLS, Zeta potential, FT-IR, and TGA analysis. GSH sensing was also studied for the GSH probe in solution, conjugated to SONPs, and in living cells, indicating promising behavior for ratiometric GSH detection.

2. Results and Discussion

2.1. Synthesis and Characterization of Functionalized Nanoparticles

The molecular probe PB was synthesized following a five steps sequence depicted in Scheme S1 (Supporting Information). Briefly, condensation of pyrrole and 4-(prop-2-yn-1-yloxy)benzaldehyde **(1)**, which was prepared by reaction of 4-hydroxybenzaldehyde and propargyl bromide, afforded the dipyrromethane **2**, which was subsequently chlorinated (**3**) and oxidized to give **4**. Then, boron trifluoride etherate was introduced in the presence of triethylamine affording the BODIPY derivative PB. All synthesized compounds were characterized by ^{1}H NMR, ^{13}C NMR, MALDI-TOF MS, and FT-IR (Figures S1–S14 in Supporting Information). For preparation of functionalized nanoparticles, pristine SONPs were functionalized with either a) an azide linker to give SONPs-N3 or b) a mixture (8:2) of the azide linker and a poly(ethylene oxide) ligand as a water dispersant to afford SONPs-N3-PEO, which were then conjugated to GSH probe PB to yield SONPs-PB-PEO (**Figure 1**a).

High-resolution transmission electron microscopy (HR-TEM) was utilized to evaluate the morphology and size of all silicon oxide nanoparticles, and images are shown in Figure 1b–d for the pristine SONPs, SONPs-N3-PEO, and SONPs-PB-PEO, respectively. Figure 1b reveals that the pristine SONPs nanoparticles have a spherical morphology with an average diameter of 57 ± 4 nm. The size distribution of SONPs nanoparticles also exhibits in Figure S15 (Supporting Information). After surface functionalization, a thin organic layer is observed around both types of nanoparticles SONPs-N3-PEO (Figure 1c) and SONPs-PB-PEO (Figure 1d), which is about 3 ± 0.2 nm, whereas there is no change in the size of the core nanoparticles. Figures S16 and S17 (Supporting Information) also show the more HR-TEM images of SONPs-N3-PEO and SONPs-PB-PEO, respectively.

The thin organic layer around the SONPs-N3-PEO corresponds to the azide end group as a linker and a poly (ethylene oxide) end chain as a dispersant. According to calculations, the length of the linkers and PB is about 3.4 nm, which is consistent with a monolayer around the SONPs after surface functionalization.

The average size of pristine SONPs in the dispersion was 112 nm (**Table 1**, Figure S18, Supporting Information), while for SONPs-PB-PEO the hydrodynamic diameter increased to 122 nm (**Figure 2**a), which confirms the presence of a monolayer around the later SONPs. The hydrodynamic diameter of SONPs-N3-PEO is also about 120 nm (Figure S18, Supporting Information) which does not show considerable change compared to SONPs-PB-PEO as the size of PB molecule is less than 1 nm. The results from DLS also exhibit that the hydrodynamic diameter of SONPs-N3 is about 476 nm, which can be explained by the aggregation of SONPs in the aqueous solution in the absence of a poly (ethylene oxide) end chain as a dispersant on the surface of nanoparticles. PEO chains conjugated to the surface of nanoparticles modify their surface properties, making them more compatible with aqueous environments. This surface modification transforms hydrophobic nanoparticles into hydrophilic ones since PEO chains are hydrophilic due to their ether oxygen atoms, which readily form hydrogen bonds with water molecules.[18] This hydrophilic nature increases the solubility of the nanoparticles in water, preventing them from aggregating and settling out of solution.[19] DLS was also measured for SONPs-PB-PEO at different time intervals in order to evaluate the long-term stability and change of hydrodynamic diameter resulting from the aggregation of nanoparticles. The hydrodynamic diameter of SONPs-PB-PEO was 123 ± 3 nm (PdI = 0.142), 125 ± 5 nm (PdI = 0.137), and

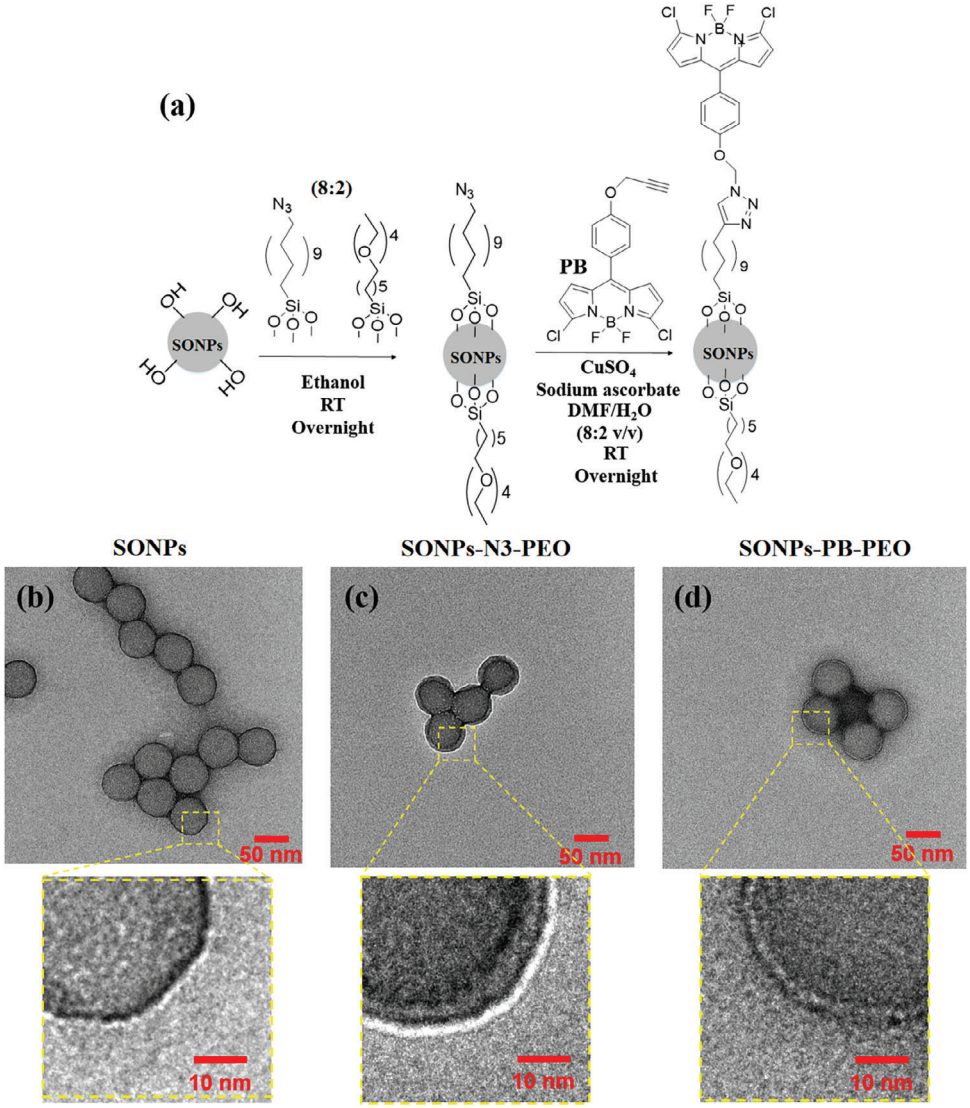

Figure 1. a) Surface functionalization process of silicon oxide nanoparticles. HR-TEM images of b) pristine SONPs and c) SONPs-N3-PEO, and d) SONPs-PB-PEO.

126±2 nm (PdI = 0.163) after 1, 3, and 7 d in dispersion (Figure S19, Supporting Information), respectively, indicating no significant change in size compared with the freshly prepared SONPs-PB-PEO dispersion.

The surface charge and stability of non-functionalized and functionalized SONPs in the aqueous solution was evaluated using zeta potential experiments. The average zeta potential value for SONPs-PB-PEO is −38±4 mV (Figure 2b), a value more negative than the threshold (±25 mV)[20] for the colloidal stability of nanoparticles. Poly (ethylene oxide) groups in the dispersant can establish hydrogen bonds with water, and consequently the dispersibility of functionalized SONPs increases, which results in higher stability in the aqueous media. The zeta potential plot for SONPs-N_3-PEO is also exhibited in Figure S20 (Supporting

Table 1. DLS (in H_2O) and zeta potential (in 6×10^{-3} M NaCl solution) values for different SONPs.

Sample (NPs)	Size[a] ± SD[b] (Diameter [nm])	PdI	Zeta potential[a] ± SD[b] [mV]
SONPs	112 ± 3	0.108	−48 ± 8
SONPs-N_3	476 ± 6	0.131	−12 ± 4
SONPs-N_3-PEO	120±3	0.142	−36 ± 5
SONPs-PB-PEO	122±2	0.153	−38 ± 4

[a] Average of $n = 3$; [b] SD = Standard deviation.

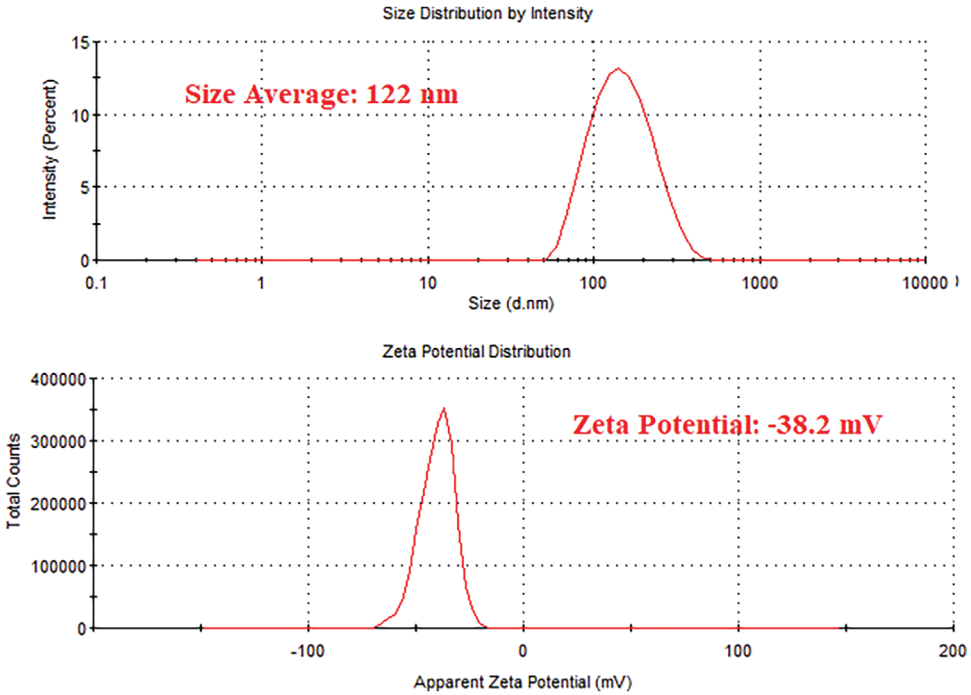

Figure 2. a) Size distribution plot and b) zeta potential plot of SONPS-PB-PEO.

Information), which shows an average value of −36 ± 5 mV. Instead, the zeta potential value of −12±4 mV for SONPs-N_3 indicates they are not stable in aqueous dispersion. When the measurement is done in ethanol, the SONPs-N3 nanoparticles (Figure S20, Supporting Information) have a value of −30 ± 3 mV, indicative of the higher stability of SONPs-N_3 nanoparticles in this solvent. To investigate the long-term colloidal stability of SONPs-N3-PEO, zeta potential was measured after 1, 3, and 7 d, showing values of 37 ± 3, 35 ± 4, and 32 ± 3 mV (Figure S21, Supporting Information), respectively. These experiments indicate that even 7 d after the preparation of SONPs-N3-PEO in dispersion, they showed excellent stability compared to the freshly prepared dispersion of SONPs-N3-PEO.

By comparing FT-IR spectroscopy of SONPs-PB-PEO (**Figure** 3a) with the ones of pristine SONPs, SONPs-N3-PEO, azide linker (Figure S22, Supporting Information), and PB molecule, it was observed that there are new peaks 1390, 1500–1625, and 2926 cm^{-1} corresponding to the conjugated PB molecules and the stretching vibration bonds of —CH are observed which correspond to the carbon chain of linkers in SONPs-PB-PEO, and there is not any evidence of azide related to linker after the conjugation reaction.

To quantify the functionalization of nanoparticles, thermogravimetric analysis (TGA) was performed (Figure 3b). For the pristine SONPs, as it can be seen, there is a mass loss of about 3.4% from the temperature of 30 °C to 150 °C, which corresponds to the blocked humidity evaporation in the total mass of pristine SONPs. From 150 °C to 800 °C, the mass loss corresponds to silanol groups existing at the surface of the pristine SONPs. The plot for SONPs-N3 also exhibits a mass loss reduction from 30 °C to 170 °C associated with the humidity evaporation. From 360 °C to 550 °C, there is a mass loss of about 5.2 wt% which corresponds to the azide linker conjugated to the surface of SONPs. The TGA plot of SONPs-N3-PEO also shows a mass loss of about 5.4 wt% from 360 to 550 °C which is associated with the decomposition of azide linker and poly (ethylene oxide) linker at the surface of SONPs. TGA plot for SONPs-PB-PEO exhibits three phases of mass loss. From 30 °C to 150 °C, the mass loss corresponds to the blocked water molecule evaporation, as this mass loss can also be seen in other samples. From 220 °C to 340 °C, a mass loss of about 4.3 wt% is seen which is related to the PB molecules. In the TGA plot of SONPs-PB-PEO, the mass loss of about 5.7 wt%, corresponding to the decomposition of linkers, is also seen from 360 °C to 550 °C. According to Equation (1) the densities of N3-PEO and PB on the surface of SONPs were calculated to be 12×10^{-6} mol m^{-2} (or 2.6 × 104 molecule per NP) and 8.2×10^{-6} mol m^{-2} (or 1.8×10^4 molecule per NP), respectively.

2.2. GSH Sensing in Solution Using the Molecular Probe PB

In order to study the sensing ability of PB, its optical properties were investigated using UV–Vis absorption spectroscopy in a mixture of PBS buffer/acetonitrile (90:10, v/v, pH = 7.4, 37 °C), at a PB concentration that showed minimum self-quenching (10×10^{-6} M), in the absence and presence of GSH. As it can be seen in **Figure** 4a,b, the maximum absorbance of PB is at $\lambda_{max} = 508$ nm. In the presence of GSH (1×10^{-3} M) the absorbance related to PB at this wavelength decreases, whereas two new peaks at $\lambda = 542$ nm and $\lambda = 572$ nm appear from 5 to 30 min and 32 to 240 min, respectively. These new peaks correspond to the generation of new chromophores[21] as a consequence of the reaction of the thiol group in GSH and PB (see Scheme S2, Supporting Information).

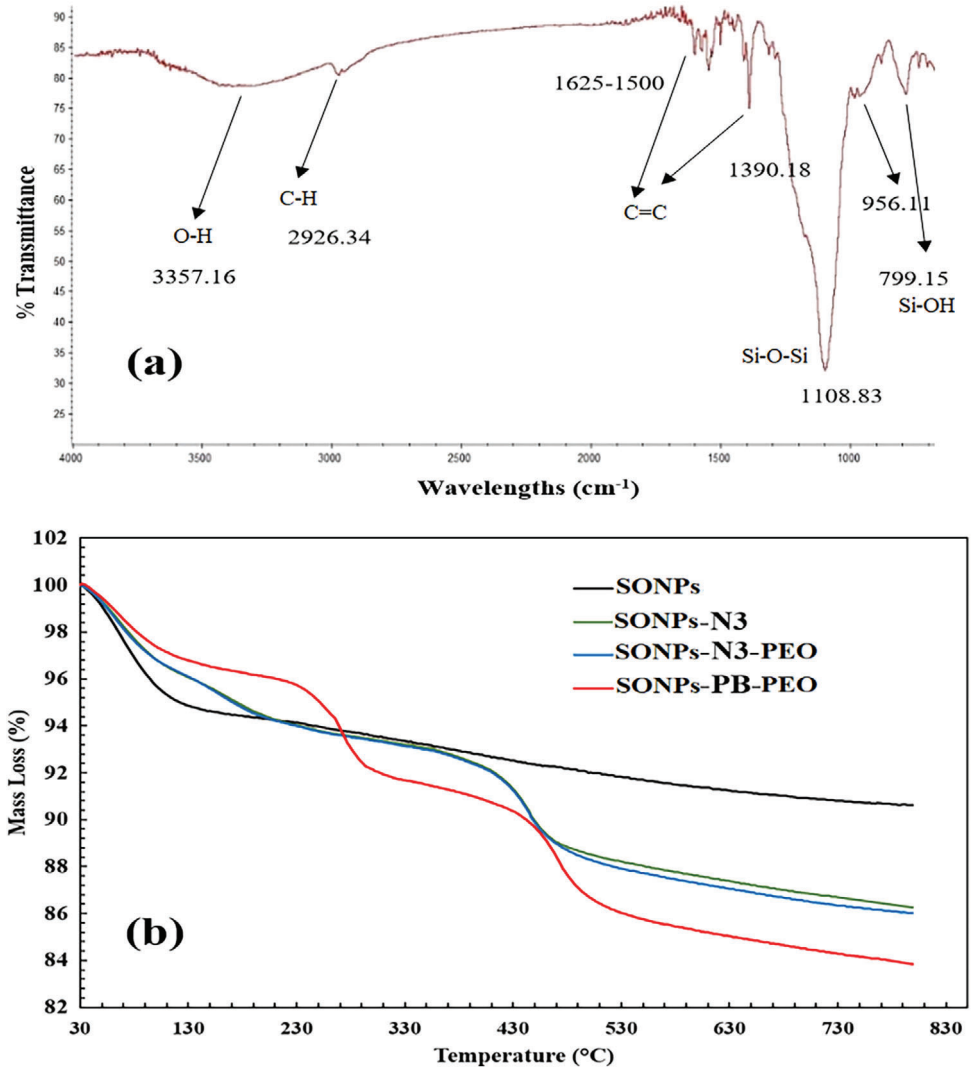

Figure 3. a) FT-IR spectrum of SONPS-PB-PEO and b) TGA plot for non-functionalized and functionalized SONPs.

Figure 4c,d shows the time-dependent fluorescence spectra from 5 to 30 min and 32 to 240 min, in which the excitation wavelength was selected at $\lambda = 508$ nm and $\lambda = 542$ nm, respectively. When PB is excited at $\lambda = 508$ nm in the absence of GSH molecules, the maximum emission is centered at $\lambda = 525$ nm. However, there was not any evidence of a recognizable peak after exciting at $\lambda = 542$ nm in the absence of GSH (data not shown). In the presence of 1×10^{-3} M GSH, there is a reduction in the emission intensity at $\lambda = 525$ nm followed by the appearance of new peaks at $\lambda = 555$ nm and $\lambda = 585$ nm which are associated with mono-substituted and di-substituted chromophores. Figure S23 (Supporting Information) shows the plots related to the kinetics of mono-substituted and di-substituted reactions. According to these plots, the mono-substitution reaction is faster ($k = 0.0877$ min^{-1}) than the di-substitution one ($k = 0.0068$ min^{-1}). To study the effect of pH on the sensitivity of the PB probe, time-dependent experiments were also conducted at pH 8, which is the mitochondrial pH. As seen in Figure S24 (Supporting Information), the mono-substitution reaction is completed after 10 min, and the fluorescence spectrum of the di-substitution reaction product at pH 8 reaches the same intensity as the fluorescence spectrum of the di-substitution reaction at pH 7.2 after 50 mi. This indicates that increasing the pH value has improved the speed of the reaction due to the conversion of the thiol group to thiolate, which is a better nucleophile. The calculated kinetics of the reactions (Figure S25, Supporting Information) also show a four-times increase in the speed of the mono-substitution reaction ($k = 0.356$ min^{-1}) and a five-times increase in the speed of the di-substitution reaction ($k = 0.356$ min^{-1}) compared to the experiments at pH 7.2. The stability of the PB probe was studied at two different pH values, 7.2 (biological pH) and 8 (mitochondrial pH), in the absence of GSH. As can be seen in Figures S26 and S27 (Supporting Information), the change in absorbance values from $t = 0$ to $t = 72$ h is negligible at both pH 7.2 and 8, indicating the stability of the PB probe under these conditions.

Figure 5a,b shows the fluorescence spectra of a 10×10^{-6} M solution of PB in the presence of different concentrations (0×10^{-6} to 50×10^{-6} M) of GSH, with excitation at $\lambda = 508$ nm. When

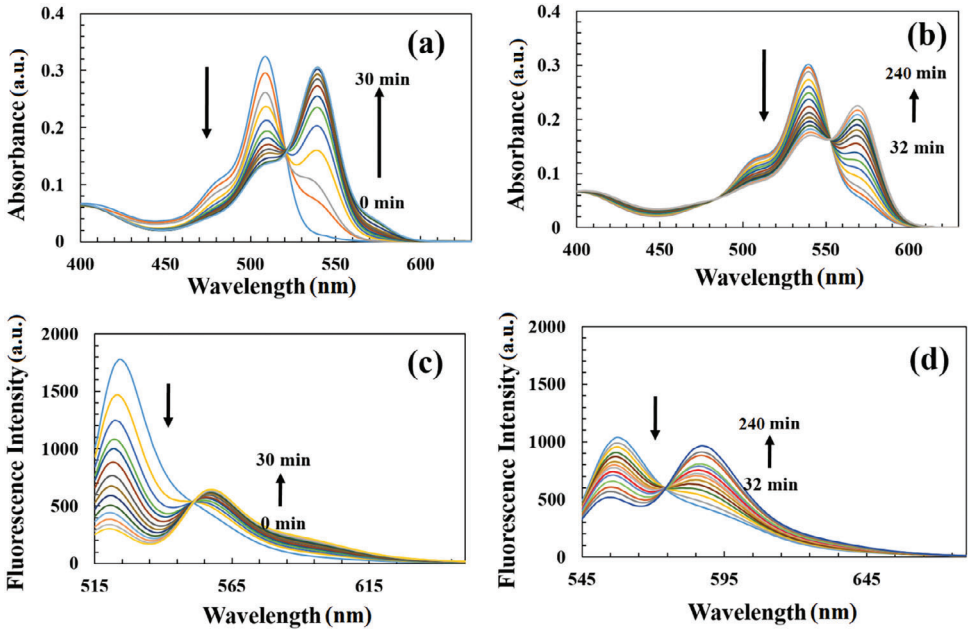

Figure 4. UV–Vis absorption spectra for 10×10^{-6} M of PB in the absence and presence of 1×10^{-3} M GSH during a) 0 to 30 min and b) 32 to 240 min. Fluorescence spectra for 10×10^{-6} M of PB in the absence and presence of 1×10^{-3} M GSH during c) 0 to 30 min and d) 32 to 240 min. (PBS: MeCN (90:10), pH = 7.2, 37 °C).

the GSH concentration is increased, there is a reduction in the fluorescence intensity at $\lambda = 525$ nm and increasing fluorescence intensity at $\lambda = 555$ nm, which is related to the mono-substituted chromophore.

Moreover, by increasing the concentration of GSH from 75×10^{-6} to 1000×10^{-6} M, there is a reduction in the emission intensity at $\lambda = 555$ and increasing emission intensity at $\lambda = 585$, which is related to the di-substituted chromophore. Figure 5c,d show the ratiometric curves associated with the GSH concentrations from 0×10^{-6} to 50×10^{-6} M and 75×10^{-6} to 1000×10^{-6} M, respectively, which are fitted to the linear behavior.

Regarding the sensitivity and selectivity of the PB probe to other biomolecules, the modification of 3,5-dichloroBODIPY with O- and N-nucleophiles has been reported in the literature,[22] illustrating that the mono- and disubstituted chromophores with O- and N-nucleophiles exhibit absorption and emission

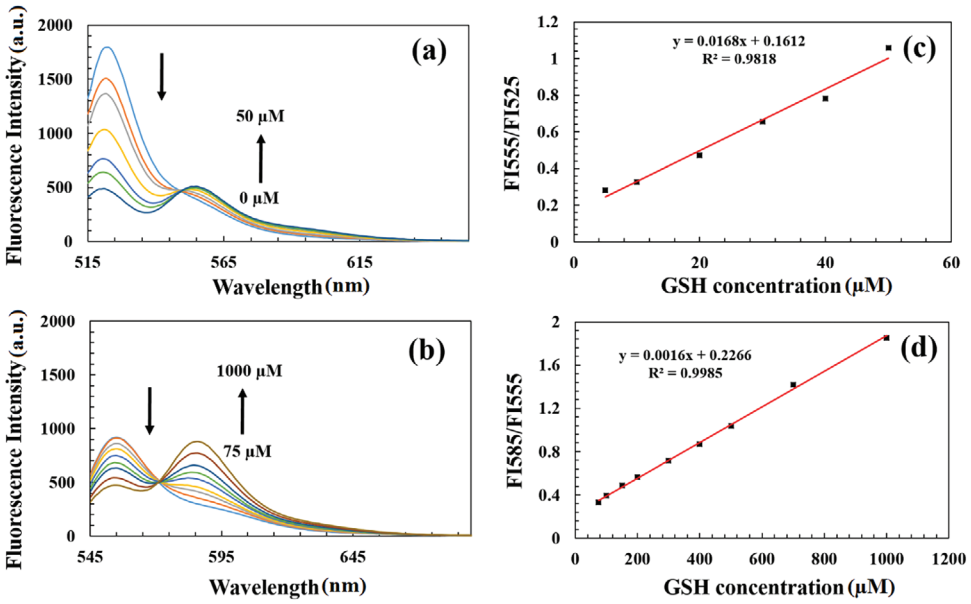

Figure 5. Fluorescence spectra for 10×10^{-6} M of PB in different concentrations of GSH from a) 0×10^{-6} to 50×10^{-6} M and c) 75 to 1000 (PBS:MeCN (90:10), pH = 7.2, 37 °C, $t = 240$ min). Ratiometric curves for b) 0×10^{-6} to 50×10^{-6} M and d) 75×10^{-6} to 1000×10^{-6} M concentrations of GSH.

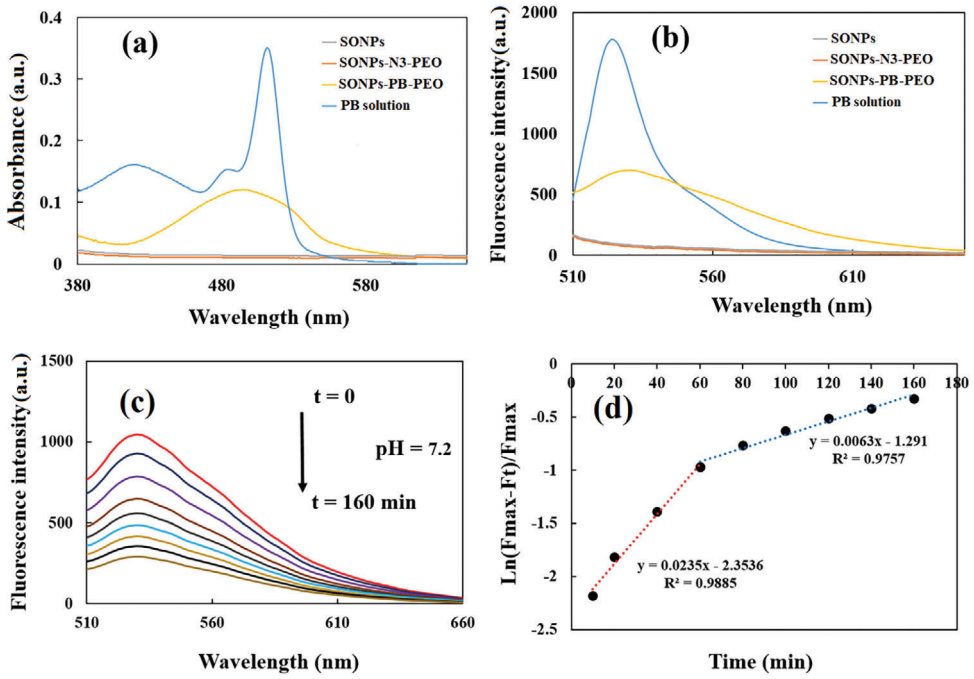

Figure 6. a) UV–Vis spectra and b) fluorescence spectra for PB, pristine SONPs, SONPs-N3-PEO, and SONPs-PB-PEO. c) Fluorescence spectra and d) kinetic study of the 0.5 mg mL^{-1} of SONPs-PB-PEO in the presence of 1×10^{-3} M GSH ((pH = 7.2, 37 °C, 160 min).

spectra in the range of 479 to 529 nm. Comparison of these results with those mentioned in the current work indicates that the PB probe exhibits good sensitivity and selectivity in biological environments.

2.3. GSH Sensing in Solution Using the SONPs-PB-PEO

Before performing in vitro sensing experiments, PB was immobilized on SONPs to overcome its lack of water solubility, cell uptake enhancement, as well as improving its biocompatibility, and the sensing behavior of SONPs-PB-PEO in aqueous dispersion was also examined. **Figure** 6a,b exhibits UV–Vis absorption and fluorescence spectra, respectively, for PB and SONPs-PB-PEO in the absence of GSH. Pristine SONPs and SONPs-N_3-PEO were included as controls. SONPs-PB-PEO shows broad absorption and emission peaks at λ = 495 nm and λ = 530 nm, respectively, which indicates the conjugation of PB on the surface of SONPs. The broad shape and a slight difference between the absorption and emission peaks of SONPs-PB-PEO compared with PB molecule can correspond to the population and polydispersity of nanoparticles in the aqueous dispersion[23] (see DLS plots in Figure S18, Supporting Information).

The sensitivity of SONPs-PB-PEO (0.5 mg mL^{-1}) toward GSH was studied during different time intervals in the presence of 1×10^{-3} M GSH molecule during 160 min and pH = 7.2. As it can be seen from Figure 6c, there is a reduction in the fluorescent intensity of SONPs-PB-PEO from t = 5 min to t = 160 min. However, the first peak related to mono-substitution is not visible. One possible reason can be associated with the broad shape of fluorescence spectra of immobilized PB on SONPs, which overlaps with the peak of mono-substituted chromophore possessing lower fluorescence intensity compared to PB molecule. Figure 6d also exhibits the kinetics calculations resulting from the time-dependent experiments SONPs-PB-PEO during the time intervals of t = 5 min to t = 160 in pH = 7.2. As it can be seen, there are two linear phases one is from t = 5 to t = 60 min and the other one is from t = 60 min to t = 160 min. From the slope of curves, it can be concluded that the interaction between GSH and SONPs-PB-PEO is faster (k = 0.0235 min^{-1}) during t = 5 to t = 60 min compared with the time interval of t = 60 to 160 min (k = 0.0063 min^{-1}) which is four times slower than the first-time intervals.

The sensitivity of SONPs-PB-PEO in the presence of GSH (1×10^{-3} M) was also studied at pH 8, which is the mitochondrial pH environment (Figure S28, Supporting Information). At this pH, the reduction in the fluorescent intensity of SONPs-PB-PEO was faster and reached to the same fluorescent intensity value after 45 min compared to the time interval of 160 min, and the kinetics calculation exhibits only one linear curve (k = 0.0387 min^{-1}). The thiol groups can be converted to thiolate which is a better nucleophile resulting in the increment of the speed of nucleophilic substitution reaction with the SONPs-PB-PEO.

The sensitivity of SONPs-PB-PEO was also studied toward different concentrations of GSH. **Figure** 7a shows the fluorescence spectra (λ_{ex} = 495 nm) of a 0.5 mg mL^{-1} aqueous dispersion of SONPs-PB-PEO in the presence of various concentrations of GSH (20×10^{-6} to 1×10^{-3} M) after 160 min, pH = 7.2, and 37 °C. An increasing concentration of GSH in the solution was related to a reduction in the fluorescence intensity at λ = 530 nm, which confirms the reaction of GSH with PB at the surface of SONPs. For the GSH concentrations of 1.5 $\times 10^{-3}$ to 3×10^{-3} M, a new peak appears in the wavelength of λ = 560 nm corresponding to the new chromophore at the surface of nanoparticles (Figure 7b). Additionally, the di-substituted peak is not visible even at higher

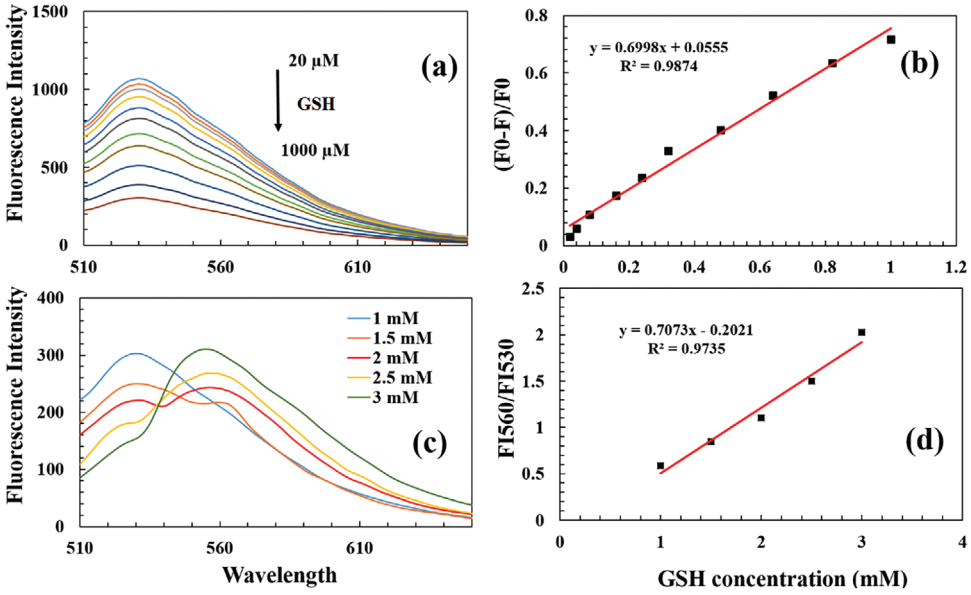

Figure 7. a) Fluorescence spectra and b) fluorescence intensity in terms of GSH enhancement of the 0.5 mg mL^{-1} of SONPs-PB-PEO in the presence of various concentrations of GSH (20×10^{-6} M to 1×10^{-3} M) (pH = 7.4, 37 °C, 160 min). c) Fluorescence spectra and d) the ratio-metric curve of the 0.5 mg mL^{-1} of SONPs-PB-PEO in the presence of various concentrations of GSH (1×10^{-3} to 3×10^{-3} M) (pH = 7.4, 37 °C, 160 min).

GSH concentrations due to steric hindrance from the spatial arrangement of molecules on the nanoparticle surface. This effect can prevent or delay reactions like nucleophilic substitution.[24] After PB immobilization on SONPs, the crowded electrophilic center and the presence of mono-substituted chromophores further prevent di-substitution.

Figure 7c,d shows the relationship between fluorescence intensity in terms of GSH enhancement for the concentrations of 20×10^{-6} to 1×10^{-3} M and the ratiometric curve for GSH concentrations of 1×10^{-3} to 3×10^{-3} M, respectively, which show linear behavior. Consequently, SONPs-PB-PEO showed desirable properties as a promising nanosensor, with the advantage of being stable in aqueous media, hence addressing the solubility issue of molecular probes for GSH detection.

3. Cellular Imaging and Cytotoxicity Assessment

Cell internalization of PB probe, as well as the possibility of detecting the alteration of intracellular GSH levels, was also studied. The blank control of HeLa cells in the absence of the PB probe and incubated only with buthionine sulfoximine (BSO), which reduces levels of glutathione in living cells,[25] showed no fluorescence emission at λ_{em} = 498–531 nm (emission range only for PB) or λ_{em} = 565–632 nm (emission range for PB+GSH) (Figure S29, Supporting Information). The cell permeability of PB was confirmed at 1×10^{-6}, 2×10^{-6}, and 5×10^{-6} M, and after 15 min incubation (Figure S30, Supporting Information). After incubation of living cells with 1×10^{-3} M of BSO for 24 h and subsequent incubation with 2×10^{-6} and 5×10^{-6} M PB, there was a reduction in the ratiometric fluorescence intensity in the presence of BSO for both 2×10^{-6} and 5×10^{-6} M concentrations of PB, indicating the sensitivity of these two concentrations to the intracellular of GSH levels alterations (Figure S30, Supporting Information). However, there were not any differences with lower concentrations of PB probe (1×10^{-6} M) in the absence and presence of BSO in cells. Ratiometric fluorescence intensity was also analyzed when cells incubated with BSO and subsequent addition of 10×10^{-3} M GSHee, which is a permeable derivate of GSH.[26] As it is observed in **Figure 8**, compared with control conditions (Figure 8a–d), the fluorescence intensity at λ_{em} = 498–531 nm increases while the intensity is reduced at λ_{em} = 565–632 nm when intracellular GSH levels decrease (Figure 8e–h). On the other hand, Figure 8i–l exhibits the increment of fluorescence intensity at λ_{em} = 565–632 nm followed by reduction at λ_{em} = 498–531 nm confirming the sensitivity of PB even in the higher level of intracellular GSH. In similar experiments with the N-ethylmaleimide (NEM), which is a GSH scavenger, the increase at λ_{em} = 498–531 nm was highly significant and this effect together with the decrease of intensity at λ_{em} = 565–632 nm was reflected in the ratiometric detection (Figure S31, Supporting Information). Also, similar to the BSO experiment, the addition of GSHee during 4 h after NEM incubation reverses the ratiometric fluorescence intensity detected in NEM conditions, confirming the sensitivity of PB probe to the alteration of intracellular GSH levels.

The cytotoxicity of SONPs-PB-PEO was also analyzed in HeLa cells using alamarBlue assay, which relies on the ability of living cells to reduce resazurin, a nonfluorescent blue dye, to resorufin, a fluorescent pink compound, through mitochondrial and cytoplasmic enzyme activity.[27] This reduction process is an indicator of metabolic activity, making it possible to quantify cell viability and cytotoxicity by measuring the resulting fluorescence or absorbance.[28] The results indicated that neither of the two concentrations of SONPs-PB-PEO used (20 and 50 μg mL^{-1}) were toxic after 4 or 48 h of incubation (**Figure 9**). The cytotoxicity of SONPs-PB-PEO was found to be identical to the cytotoxicity induced by SONPs alone (data not shown). The cytotoxicity

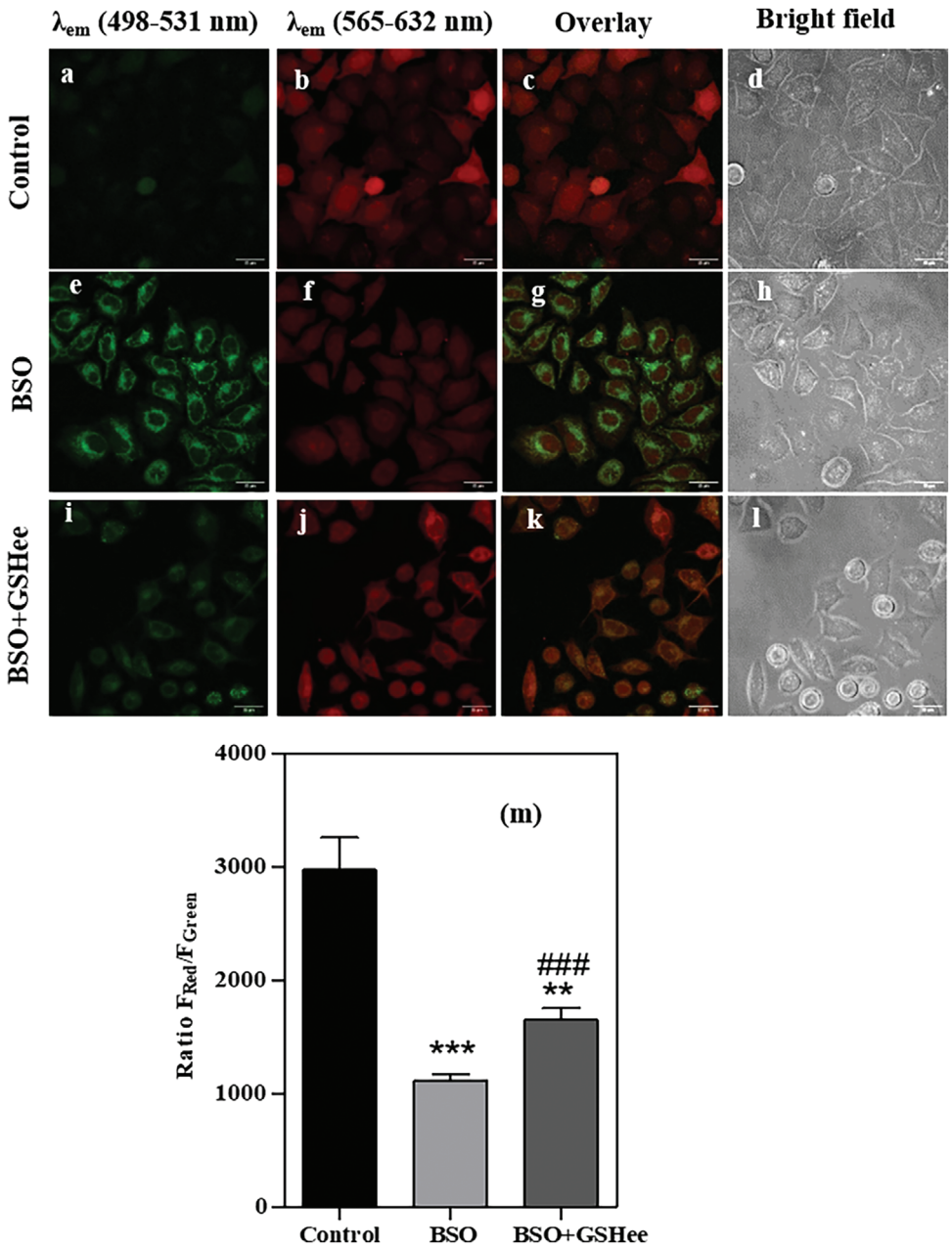

Figure 8. Representative confocal images of HeLa cells in the presence of 5×10^{-6} M PB and incubation time of 15 min in different conditions: a–d) control, e–h) 24 h incubation with 1×10^{-3} M BSO, and i–l) BSO condition followed by 4 h incubation with 10×10^{-3} M of GSHee. m) The ratiometric analysis of individual cells in independent experiments. ($n = 67–76$ cells). Statistical analysis was performed by One-way ANOVA. * compared control versus BSO or BSO+GSHee; # compared BSO+GSHee versus BSO. ***,###$p < 0.001$, **$p < 0.01$.

results reveal excellent biocompatibility of SONPs-PB-PEO, even for long-term applications.

4. Conclusion

We have synthesized and characterized the optical properties of a new ratiometric fluorescent molecular probe, PB, for sensing GSH. This probe is formed by three moieties: a) a fluorescent moiety, which is a BODIPY core, b) chlorine substituents for reaction with GSH, and c) a propargyloxy moiety at the para position of the meso phenyl substituent for conjugation to the SONPs. The conjugation of PB to the surface of SONPs was successfully achieved, and multifunctionalized SONPs-PB-PEO were characterized with relevant techniques. HR-TEM images exhibited a thin layer around SONPs-PB-PEO, which was about 3 ± 0.2 nm, corresponding to conjugated PB and linker to the surface of SONPs. FT-IR spectra also confirmed the surface functionalization of nanoparticles. Using TGA analysis, the densities of linkers and PB on the surface of SONPs were calculated. SONPs-PB-PEO exhibited considerable stability in aqueous

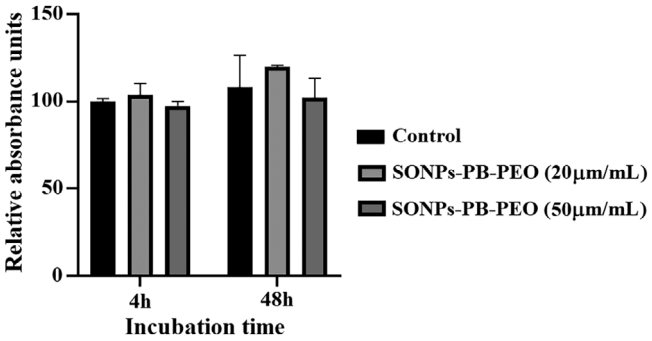

Figure 9. The graph represents the relative absorbance detected with alamarBlue reagent after incubation with 20 μg mL^{-1} and 50 μg mL^{-1} of SONPs-PB-PEO for 4 or 48 h, compared with the data after 4 h without SONPs-PB-PEO (control).

dispersion without the need for an organic solvent, which is an advantage of these nanoparticles compared to PB for GSH detection. The sensitivity of PB in the solution and at the surface of SONPs-PB-PEO was confirmed, resulting in ratiometric linear trends. Although SONPs-PB-PEO exhibited good sensitivity to different concentrations of GSH, after immobilization of PB to the surface of SONPs, the crowded electrophilic center and the presence of mono-substituted chromophores prevent further di-substitution. As a result, only one new emission peak appears for detecting GSH, which can make the detection of GSH easier, especially at higher GSH concentrations, instead of the two new emission peaks seen with the PB molecule alone in different concentrations of GSH. PB demonstrated a satisfactory performance in detecting intracellular changes in GSH levels, indicating a promising use of the conjugated water-dispersible nanoparticles with PB for future investigations. Moreover, the cytotoxicity results demonstrate that SONPs-PB-PEO exhibits excellent biocompatibility, making it suitable for long-term applications.

5. Experimental Section

Materials: 4-Hydroxybenzaldehyde, propargyl bromide, pyrrole, trifluoroacetic acid (TFA), *N*-chlorosuccinimide, p-chloranil, triethylamine, boron trifluoride etherate, potassium carbonate, phosphate buffered saline (PBS), sodium ascorbate, $CuSO_4$ and deuterated chloroform ($CDCl_3$) were purchased from Sigma-Aldrich. Acetonitrile (MeCN), tetrahydrofuran (THF), dichloromethane (DCM), toluene, hexane, and ethyl acetate were purchased from VWR Chemicals. The water used in the experiments was HPLC grade, produced by a MilliQ plus system from Millipore (Milli-Q water). Coated F_{254} silica gel plates for thin layer chromatography (TLC) were purchased from Merk Co. were applied. Silica gel (40–60 μm, VWR CHEMICALS Co.) was used for column chromatography. Pristine silicon nanoparticles (SONPS) were purchased from Alpha Nanotech Inc. 11-Azidoundecyltriethoxysilane and (6-{2-[2-(2-methoxyethoxy)ethoxy]ethoxy}hexyl)trimethoxy-silane were purchased from Sikemia.

General Methods: A Varian Mercury 400 MHz spectrometer was used for recording ^{1}H NMR (400 MHz). A Varian Mercury 400 MHz spectrometer was used for recording ^{13}C NMR (100 MHz). Thermo Nicolet Avatar 320 FTIR was also applied for the FT-IR. FT-IR samples were prepared by dissolving a sufficient quantity of the samples in chloroform ($CHCl_3$), then adding one drop of the solution to a NaCl disk (round crystal window, NaCl, diameter = 25 mm, thickness = 4 mm). After waiting for the solvent to evaporate, the sample was run in the equipment. MALDI-TOF analyses were performed using an LC/MSD-TOF mass spectrometer (Agilent Technologies, 2006). High-resolution transmission electron microscopy (FEI Tecnai G2 F20 200 kV) was employed for the TEM image. ImageJ[29] software was used for the characterization of the HR-TEM images. Dynamic light scattering (DLS) (0.5 mg mL^{-1} of nanoparticles in Milli-Q water) and zeta potential analysis (0.5 mg mL^{-1} of nanoparticles in 6×10^{-3} M NaCl solution, 25 °C) were also applied to study the size distribution and the surface charge of nanoparticles by the utilization of Zeta Sizer Nano series (Malvern Co.). The thermal gravimetric analyzer (Mettler-Toledo TGA-851e thermobalance) was utilized to measure the density of functional groups on the surface of SONPS under a dry nitrogen atmosphere with 50 mL min^{-1} flow rate and heating rate of 10 °C min^{-1}.

UV–vis absorption and fluorescence experiments were performed using UV-1800 Shimadzu UV and Hitachi F-4500 fluorescence spectrophotometers, respectively. Absorption quartz cuvettes (Hellma absorption cuvettes, standard cells, Macro) and fluorescence quartz cuvettes (Hellma fluorescence cuvettes, standard cells, Macro) were used for UV–vis absorption and fluorescence experiments, respectively. For these experiments, PB was prepared at a concentration of 10×10^{-6} M with a solvent proportion of PBS (90:10), pH 7.2, and a constant temperature of 37 °C. To study PB in the presence of GSH, the concentration was adjusted to 10×10^{-6} M of PB and different concentrations of GSH with a solvent proportion of PBS (90:10), pH 7.2, and a constant temperature of 37 °C. SONPs-PB-PEO was also prepared at a concentration of 0.5 mg mL^{-1} in aqueous dispersion at pH 7.2 and a constant temperature of 37 °C for analyzing the photophysical properties of functionalized nanoparticles. To study the capability of SONPs-PB-PEO in GSH sensing, the SONPs-PB-PEO aqueous dispersion (0.5 mg mL^{-1}) was adjusted to different concentrations of GSH at pH 7.2 and a constant temperature of 37 °C.

*Synthesis of GSH Probe (PB)—4-(Prop-2-yn-1-yloxy)benzaldehyde (**1**)*: 4-Hydroxybenzaldehyde (2.00 g, 16.37 mmol) was added to a 250 mL round bottom flask equipped with a magnetic stirrer and dissolved in 150 mL of dry acetonitrile. 2.9 g (24.5 mmol) of propargyl bromide was added to the solution under an Ar atmosphere. Afterward, potassium carbonate (2.5 g, 18.1 mmol) was added to the reaction. The reaction was refluxed and the progress of the reaction was monitored by TLC using DCM as the eluent. After 2 h, the reaction was completed and the mixture was cooled to room temperature. Potassium carbonate was removed from the mixture of the reaction by filtration and washed with acetonitrile (5 mL). The solvent was evaporated under vacuum, resulting in 2.33 g of **1** as a yellowish solid (yield: 89%). Melting Point: 74–76 °C. ^{1}H NMR (400 MHz, $CDCl_3$): 9.88 (s, 1H), 7.87 (d, J = 8.8 Hz, 2H), 7.13 (d, J = 8.8 Hz, 2H), 4.84 (d, J = 2.4 Hz, 2H), 2.86 (t, J = 2.4 Hz, 1H). ^{13}C NMR (100 MHz, $CDCl_3$): 55.9, 76.4, 77.5, 115.2, 130.6, 131.8, 162.4, 190.7.

*Synthesis of GSH Probe (PB)—5-(4-(Prop-2-yn-1-yloxy) phenyl)dipyrromethane (**2**)*: Compound **1** (2 g, 12.5 mmol) was added to freshly distilled pyrrole (67.1 g, 500 mmol) under Ar atmosphere and was dissolved with the aid of magnetic stirring. TFA (0.143 g, 1.25 mmol) was added dropwise to the solution, using a syringe, and the mixture was stirred for 3 h at room temperature. Subsequently, the solution was diluted with 100 mL of dichloromethane. In order to quench the TFA, 20 mL of NaOH solution (0.8 N) was added to the solution. The organic phase was separated and the aqueous phase was extracted with dichloromethane (3 × 10 mL), and the combined organic phases were dried using $MgSO_4$. Then, dichloromethane and excess pyrrole were evaporated under reduced pressure giving a residue which was purified by column chromatography with a solvent mixture containing cyclohexane (79.5%), ethyl acetate (19.5%), and TEA (1%)., resulting in 2.48 g of **2** (yield: 72%). ^{1}H NMR (400 MHz, $CDCl_3$): 7.92 (s, 2H), 7.15 (d, J = 8.4 Hz, 2H), 6.93 (d, J = 8.8 Hz, 2H), 6.69 (d, J = 1.6 Hz, 2H), 6.16 (d, J = 3.4 Hz, 2H), 5.91 (d, J = 1.5 Hz, 2H), 5.44 (s, 1H), 4.68 (d, J = 2.3 Hz, 2H), 2.51 (t, J = 2.4 Hz, 1H). ^{13}C NMR (100 MHz, $CDCl_3$): 43.1, 55.8, 75.5, 78.6, 107.1, 108.40, 114.9, 117.1, 129.4, 132.7, 135.2, 156.5.

*Synthesis of GSH Probe (PB)—1,1′-Dichloro-5-(4-(prop-2-yn-1-yloxy)phenyl)dipyrromethane (**3**)*: 0.75 g of **2** (2.7 mmol) were dissolved in dry THF (40 mL). After purging with Ar, the solution was cooled to −78 °C. Then, a suspension of *N*-chlorosuccinimide (760 mg, 5.7 mmol) in dry THF (8 mL) was added to the cooled solution. The reaction

mixture was stirred at −78 °C for 2 h and placed in the freezer overnight at −20 °C. For quenching *N*-chlorosuccinimide, 40 mL of water was added to the cold reaction mixture. The organic layer was extracted with dichloromethane (3 × 20 mL) and dried using $MgSO_4$. Afterward, the organic solvents were evaporated under reduced pressure. The residue was chromatographed with a mixture of solvents (Hexane (65%)/DCM (35%)) as eluent, resulting in 0.52 g **3** (yield: 55%). ^{1}H NMR (400 MHz, $CDCl_3$): 7.80 (s, 2H), 7.13 (d, J = 8.7 Hz, 2H), 6.95 (d, J = 8.6 Hz, 2H), 5.96 (dd, J = 3.6, 2.6 Hz, 2H), 5.82 (dd, J = 3.7, 2.9 Hz, 2H), 5.26 (s, 1H), 4.69 (d, J = 2.3 Hz, 2H), 2.53 (t, J = 2.4 Hz, 1H). ^{13}C NMR (100 MHz, $CDCl_3$): 43.7, 55.8, 75.7, 78.5, 106.4, 108.5, 113.6, 115.2, 129.4, 131.4, 133.7, 156.8. MALDI-TOF: $[M+H]^+$ 345.0413.

Synthesis of GSH probe (PB)—1,9-Dichloro-5-(4-(prop-2-yn-1-yloxy)phenyl)dipyrromethene (***4***): A suspension of p-chloranil (0.37 g, 1.51 mmol) in dichloromethane (3 mL) was added to a solution of **3** (0.52 g, 1.51 mmol) in dichloromethane (10 mL) under Ar atmosphere. The reaction mixture was stirred overnight at room temperature. After solvent evaporation, the residue was chromatographed (silica gel) by a mixture of solvents (DCM (80%)/hexane (20%)) as eluent which resulted in 0.32 g **4** (yield: 61%). Melting point: 105–108 °C. ^{1}H NMR (400 MHz, $CDCl_3$): 7.39 (d, J = 8.9 Hz, 2H), 7.05 (d, J = 8.8 Hz, 2H), 6.58 (d, J = 4.3 Hz, 2H), 6.27 (d, J = 4.3 Hz, 2H), 4.77 (d, J = 2.4 Hz, 2H), 2.58 (t, J = 2.4 Hz, 1H). ^{13}C NMR (100 MHz, $CDCl_3$): 55.9, 75.9, 78.1, 114.2, 116.8, 128.6, 130.1, 132.4, 138.5, 139.6, 141.5, 158.6. MALDI-TOF: $[M+H]^+$ 343.0417.

Synthesis of GSH Probe (PB)—4,4-Difluoro-8-(4-(prop-2-yn-1-yloxy)phenyl)−3,5-dichloro-4-bora-3a,4a-diaza-s-indacene (PB): 0.24 g (0.7 mmol) of **4** was dissolved in toluene (10 mL) and solution was purged with Ar. Then, triethylamine (1.023 g, 7 mmol) was added to the solution and the mixture was heated at 70 °C for 30 min. Afterwards, boron trifluoride etherate (1.49 g, 10.5 mmol) was added dropwise to the mixture of reaction, which was monitored by TLC. After 2 h, the reaction was completed and the mixture was cooled down to room temperature. For quenching the boron trifluoride etherate, 10 mL of 1 M aqueous solution of NaOH were added to the mixture of reaction. Then, 1 M HCl solution (2 mL) was added to the mixture to bring the pH of the solution to 6. The organic phase was extracted with dichloromethane, and the solvents were evaporated under residue pressure. The residue was chromatographed with dichloromethane as the eluent, resulting in 0.173 g of PB as a red solid. (Yield: 63%). Melting point: 175–178 °C. ^{1}H NMR (400 MHz, $CDCl_3$): 7.47 (d, J = 8.6 Hz, 2H), 7.13 (d, J = 8.7 Hz, 2H), 6.88 (d, J = 4.3 Hz, 2H), 6.44 (d, J = 4.4 Hz, 2H), 4.79 (d, J = 2.4 Hz, 2H), 2.59 (t, J = 2.4 Hz, 1H). ^{13}C NMR (100 MHz, $CDCl_3$): 55.97, 76.3, 77.8, 115.1, 118.1, 125.6, 131.5, 132.2, 133.6, 143.8, 144.3, 159.9. MALDI-TOF: $[M+H]^+$ 391.0411, $[M+NH_4]^+$ 408.0674.

Silanization of SONPS with 11-Azidoundecyltriethoxysilane (SONPS-N_3): Pristine SONPS (100 mg) were added to absolute ethanol (2.5 mL) and dispersed using an ultrasonic bath, and 11-Azidoundecyltriethoxysilane (27.7 mg, 0.087 mmol) was also dissolved in absolute ethanol (2.5 mL). The two solutions were mixed and ultrasonicated bath for 30 min. Then, the mixture of reaction was stirred at 65 °C for 48 h. After this time, the reaction was stopped and the mixture was centrifuged at 12 000 rpm for 15 min. Functionalized nanoparticles were washed with ethanol (4×1 mL) to remove the unreacted reagents and kept in absolute ethanol in fridge.

Silanization of SONPS with 11-Azidoundecyltriethoxysilane and (6-{2-[2-(2-Methoxy-ethoxy)ethoxy]-ethoxy}-hexyl)trimethoxysilane (SONPS-N3-PEO): Pristine SONPS (100 mg) was added to absolute ethanol (5 mL) and dispersed using an ultrasonic bath followed by adding 22.2 mg (0.069 mmol) of 11-azidoundecyltriethoxysilane and 6.4 mg (0.017 mmol) of (6-{2-[2-(2-methoxy-ethoxy)ethoxy]-ethoxy}-hexyl)trimethoxysilane to the mixture. The mixture of reaction was serried at 65 °C for 48 h and the reaction was stopped and centrifuged at 12 000 rpm for 15 min. Functionalized nanoparticles were washed with ethanol (4 × 1 mL) to remove the unreacted reagents and kept in ethanol in fridge.

Conjugation of PB to SONPS-N_3-PEO: 50 mg of SONPS-N3-PEO was added to a solution of DMF: H_2O (8:2 v/v) (2.5 mL), containing 1×10^{-3} M of PB (0.97 mg, 2.5×10^{-3} M), 0.1×10^{-3} M $CuSO_4$ (0.04 mg, 2.5×10^{-4} mM), and 1×10^{-3} M sodium ascorbate (0.5 mg, 2.5×10^{-3} mM). The mixture was dispersed by the ultrasonic bath for 30 min followed by stirring (450 rpm) for 24 h at room temperature. Then, the reaction was stopped and centrifuged at 12 000 rpm for 15 min followed by removing supernatant and washing (5 × 1 mL) conjugated nanoparticles with the same solvent used for reaction. SONPs-PB-PEO was dispersed in water and kept in fridge for further experiments.

Quantification of Functional Groups at the Surface of Nanoparticles: Thermogravimetric analysis (TGA) was used to measure the density of functional groups on the surface of SONPS under a nitrogen atmosphere at a heating rate of 10 °C min− from 30 to 800 °C. The surface density of functional groups was calculated by the equation below:[30]

$$c_{(\text{functional groups})} = \frac{\text{Mass loss}\%_{(\text{functional group})} / M_{(\text{functional group})}}{\frac{s}{m}} \quad (1)$$

where $c_{(\text{functional groups})}$ is the density of functional groups on the surface of SONPS, mass loss% is the mass loss of specific functional groups from 30 to 800 °C, and M(functional groups) is the functional groups' molar mass. The specific surface area of SONPS was calculated by Equation S2 (Supporting Information).

$$\frac{s}{m} = \frac{6}{\rho \times D} \quad (2)$$

where ρ is the mass density of SONPS, and D is the average diameter of SONPS. The specific surface area of SONPS with functional groups was calculated as that of pristine SONPS.

Cell Culture Condition and Probe Incubation: HeLa cell line (CCL-2) was derived from ATCC and was cultured in standard DMEM medium with 10% bovine serum buffered at physiological pH 7.4, at 37 °C with 5% CO_2. When needed, L-buthionine sulfoximine (BSO, B2515; MERCK) was added at a concentration of 1×10^{-3} M for 20–24 h; glutathione reduced ethyl ester (GSHee, G1404; Sigma-Aldrich), at a concentration of 10×10^{-3} for 4 h, and N-ethylmaleimide (NEM, 203030; ThermoScientific, Pierce) was added for 30 min, at 100×10^{-6} M. After incubations, cells were washed with PBS and PB was added at concentrations of 1×10^{-6}, 2×10^{-6} or 5×10^{-6} M in PBS and incubated for 15 min at 37 °C. After the incubation time was completed, the cells were washed with PBS, growth medium was added and then cells were observed under the microscope.

Confocal Microscopy and Image Processing: Cells were observed and images were taken under a LEICA TCS SP8 STED 3X (Leica Microsystems GmbH). Fluorescence excitation and emission of the probes were observed under CLSM at the expected windows. 8-bit images were acquired with a 63x immersion objective and a 1x optic zoom. All the images were acquired in the same conditions, with a z-step set at 1 µm. Laser intensity was adjusted to obtain all images in the fluorescence linear range and photomultiplier tube (PMT) gain and offset were optimized so the images never showed saturated pixels.

CLSM images of maximal projections were processed using the ImageJ[29] software. Ratiometric analysis of the total fluorescence intensity of red ($\lambda_{\text{excitation}}$ = 560, $\lambda_{\text{emission}}$ = 565−632 nm) and green channel ($\lambda_{\text{excitation}}$ = 488 nm, $\lambda_{\text{emission}}$ = 498−531 nm) was corrected by cell number. To have more accurate measurements, ROIs (regions of interest) corresponding to individual cells were selected and ROI quantification was performed in the same way.

Cytotoxicity Assessment: The cytotoxicity of functionalized silicon nanoparticles (SONPs-PB-PEO) was evaluated with the alamarBlue assay (DAL1025, Thermo Fisher Scientific) following the manufacturer's instructions. HeLa cells were incubated with two different concentrations of nanoparticles (20 µg mL^{-1} and 50 µg mL^{-1} of SONPs-PB-PEO). The cytotoxicity was analyzed at 4 h (short-term) and 48 h (long-term), and the data were compared with the results at 4 h without SONPs-PB-PEO (control).

Supporting Information

Supporting Information is available from the Wiley Online Library or from the author.

Acknowledgements

Project PID2020-115663GB-C3 was funded by MCIN/AEI/10.13039/5011-00011033. The authors also thank AGAUR (Generalitat de Catalunya) for a grant to consolidated research groups 2021 SGR 01085. S.B. thanks Generalitat de Catalunya for a predoctoral FISDUR scholarship. The authors also thank Dr. Thais Fedatto Abelha (Universitat de Barcelona) and Dr. Òscar Domènech (Universitat de Barcelona) for helping with access to the spectrophotometer.

Conflict of Interest

The authors declare no conflict of interest.

Data Availability Statement

The data that support the findings of this study are available in the Supporting Information of this article.

Keywords

chlorinated BODIPY scaffold, fluorescent silicon oxide nanoparticles, glutathione sensing, surface functionalization, water-dispersible nanoparticles

Received: June 13, 2024
Revised: August 1, 2024
Published online: August 12, 2024

[1] H. J. Forman, H. Zhang, A. Rinna, *Mol. Aspects Med.* **2009**, *30*, 1.
[2] M. Işık, R. Guliyev, S. Kolemen, Y. Altay, B. Senturk, T. Tekinay, E. U. Akkaya, *Org. Lett.* **2014**, *16*, 3260.
[3] C. D. Rae, S. R. Williams, *Anal. Biochem.* **2017**, *529*, 127.
[4] M. Hanko, Ľ. Švorc, A. Planková, P. Mikuš, *Anal. Chim. Acta* **2019**, *1062*, 1.
[5] J. Zhang, N. Wang, X. Ji, Y. Tao, J. Wang, W. Zhao, *Chem* **2020**, *26*, 4172.
[6] L. Zhai, Z. Shi, Y. Tu, S. Pu, *Dyes Pigm.* **2019**, *165*, 164.
[7] S. Y. Lim, K. H. Hong, D. Il Kim, H. Kwon, H. J. Kim, *J. Am. Chem. Soc.* **2014**, *136*, 7018.
[8] N. Boens, B. Verbelen, M. J. Ortiz, L. Jiao, W. Dehaen, *Coord. Chem. Rev.* **2019**, *399*, 213024.
[9] S. Bagherpour, L. Pérez-García, *J. Mater. Chem. B* **2024**, https://doi.org/10.1039/D4TB01114G.
[10] L. Baù, P. Tecilla, F. Mancin, *Nanoscale* **2011**, *3*, 121.
[11] Z. Song, F. Quan, Y. Xu, M. Liu, L. Cui, J. Liu, *Carbon* **2016**, *104*, 169.
[12] S. Jafari, H. Derakhshankhah, L. Alaei, A. Fattahi, B. S. Varnamkhasti, A. A. Saboury, *Biomed. Pharmacother.* **2019**, *109*, 1100.
[13] D. Kim, K. Shin, S. G. Kwon, T. Hyeon, *Adv. Mater.* **2018**, *30*, 1802309.
[14] X. Wen, Y. Su, G. Liu, S. Li, A. J. Müller, S. K. Kumar, D. Wang, *Macromolecules* **2021**, *54*, 1870.
[15] B. Lin, S. Zhou, *Prog. Org. Coat.* **2017**, *106*, 145.
[16] C. Morelli, P. Maris, D. Sisci, E. Perrotta, E. Brunelli, I. Perrotta, M. L. Panno, A. Tagarelli, C. Versace, M. F. Casula, F. Testa, S. Andò, J. B. Nagy, L. Pasqua, *Nanoscale* **2011**, *3*, 3198.
[17] C. von Baeckmann, R. Guillet-Nicolas, D. Renfer, H. Kählig, F. Kleitz, *ACS Omega* **2018**, *3*, 17496.
[18] Y. Aray, M. Marquez, J. Rodríguez, D. Vega, Y. Simón-Manso, S. Coll, C. Gonzalez, D. A. Weitz, *J. Phys. Chem. B* **2004**, *108*, 2418.
[19] S. Donets, J.-U. Sommer, *J. Phys. Chem. B* **2018**, *122*, 392.
[20] A. J. Shnoudeh, I. Hamad, R. W. Abdo, L. Qadumii, A. Y. Jaber, H. S. Surchi, S. Z. Alkelany, in *Biomaterials and Bionanotechnology* (Ed: R. K. Tekade), Academic Press, Cambridge, MA **2019**, pp. 527–612.
[21] L. Y. Niu, Y. S. Guan, Y. Z. Chen, L. Z. Wu, C. H. Tung, Q. Z. Yang, *J. Am. Chem. Soc.* **2012**, *134*, 18928.
[22] T. Rohand, M. Baruah, W. Qin, N. Boens, W. Dehaen, *Chem. Commun.* **2006**, 266.
[23] E. Tomaszewska, K. Soliwoda, K. Kadziola, B. Tkacz-Szczesna, G. Celichowski, M. Cichomski, W. Szmaja, J. Grobelny, *J. Nanomater.* **2013**, *2013*, 313081.
[24] M. Gallegos, A. Costales, Á. M. Pendás, *J. Comput. Chem.* **2022**, *43*, 785.
[25] R. Drew, J. O. Miners, *Biochem. Pharmacol.* **1984**, *33*, 2989.
[26] F. Magata, A. Ideta, F. Matsuda, M. Urakawa, Y. Oono, *Theriogenology* **2021**, *167*, 37.
[27] S. Uzunoglu, B. Karaca, H. Atmaca, A. Kisim, C. Sezgin, B. Karabulut, R. Uslu, *Toxicol. Mech. Methods* **2010**, *20*, 482.
[28] E. M. Longhin, N. El Yamani, E. Rundén-Pran, M. Dusinska, *Front. Toxicol.* **2022**, *4*, 981701.
[29] C. A. Schneider, W. S. Rasband, K. W. Eliceiri, *Nat. Methods* **2012**, *9*, 671.
[30] M. Li, F. Cheng, C. Xue, H. Wang, C. Chen, Q. Du, D. Ge, B. Sun, *Langmuir* **2019**, *35*, 14688.

